



Shahid Chamran  
University of Ahvaz

# Journal of Applied and Computational Mechanics



Research Paper

## Analysis of Dual Solutions of Unsteady Micropolar Hybrid Nanofluid Flow over a Stretching/Shrinking Sheet

Nepal Chandra Roy<sup>1</sup>, Md. Anwar Hossain<sup>2</sup>, Ioan Pop<sup>3</sup>

<sup>1</sup> Department of Mathematics, University of Dhaka, Dhaka, 1000, Bangladesh, Email: nepal@du.ac.bd

<sup>2</sup> Department of Mathematics, University of Dhaka, Dhaka, 1000, Bangladesh, Email: anwar.cfd@gmail.com

<sup>3</sup> Department of Applied Mathematics, Babeş-Bolyai University, Cluj-Napoca, Romania, Email: popm.ioan@yahoo.co.uk

Received August 18 2020; Revised September 11 2020; Accepted for publication September 11 2020.

Corresponding author: Ioan Pop (popm.ioan@yahoo.co.uk)

© 2020 Published by Shahid Chamran University of Ahvaz

**Abstract.** An unsteady boundary layer flow of a micropolar hybrid nanofluid over a stretching/shrinking sheet is analyzed. The nonlinear ordinary differential equations of the problem have been solved using the efficient implicit Runge-Kutta-Butcher method along with Nachtsheim-Swigert iteration technique. For a certain set of parameters, numerical results expose dual solutions with the change of the velocity ratio parameter. The dual solutions are presented in a wide range of the physical parameters. Using a lot of numerical data, the critical values of the velocity ratio parameter, local friction factor, local couple-stress and local Nusselt number for the existence of dual solutions are expressed as a function of the physical parameters. These expressions might be useful for the development of new technology or for the future experimental investigation.

**Keywords:** Dual solutions; Micropolar fluid; Hybrid nanofluid; Stretching or shrinking sheet.

### 1. Introduction

Heat transfer augmentation of micropolar fluids has been considered by many researchers because of the use of such kind of fluids in industrial and technological applications. Over decades, the thermal performance of the traditional fluids is enhanced by dispersing nanoparticles into it and the resulting fluid is known as nanofluids. As the thermal conductivity of the nanoparticles is high, the effective thermal conductivity of the nanofluids is thus higher than the base fluid. In this way, the nanofluids yield pronounced heat transfer compared to the base fluid. Since this branch of fluid dynamics is still not matured, there are a lot of problems to be investigated. Izadi et al. [1] studied the heat transfer characteristics of micropolar nanofluid inside an enclosure taking into account the effect of magnetic field on the dynamic viscosity. Contrary to this, Hashemi et al. [2] investigated the influences of heat generation and nanoparticles in a micropolar fluid within an enclosure. Later, Hashemi et al. [3] examined the natural convective flow of micropolar nanofluid inside an enclosure embedded in a porous medium considering magnetic field and thermal radiation.

Bourantas and Loukopoulos [4] focused on the heat transfer characteristics of natural convection flow of a micropolar nanofluid in a square cavity. They mentioned that the rotation of nanoparticles noticeably affects the heat transfer and flow field. Moreover, Bourantas and Loukopoulos [5] extended the model to study the magnetic effect on the natural convective heat transfer of a micropolar nanofluid in an inclined rectangular cavity. They found that the flow and heat transfer were influenced by the intensity and direction of the magnetic field. Lok et al. [6] analyzed the unsteady features of a micropolar fluid flow towards a flat surface. The flow properties are illustrated for different values of the time and the skin friction coefficient is shown in the change of the coupling parameter. Results revealed that when strong concentration of microelements is considered the boundary layer separation takes place for a larger value of the coupling parameter, however, when weak concentration of microelements is adopted the boundary layer separates from the surface for all values of the coupling parameter. The flow and heat transfer of mixed convection flow toward a vertical surface was studied by Lok et al. [7]. A linearly varying temperature is assumed along the surface. They found that the dual solutions exist for opposing flow in a certain region of the mixed convection parameter.

The boundary layer characteristics over a stretching/shrinking sheet has received attention of researchers because of its similarities with numerous engineering and industrial applications. Hussain et al. [8] examined the stagnation point flow of micropolar nanofluids over a stretching sheet. Patel et al. [9] considered the micropolar nanofluid over a stretching/shrinking sheet in the presence of thermal radiation and magnetic field. Hussanan et al. [10] investigated the convective heat transfer of micropolar nanofluids from a vertical surface. Ishak et al. [11] studied the boundary layer characteristics of a micropolar fluid past over the parallel or reverse moving surfaces relative to the free stream. Bhattacharyya et al. [12] examined the flow behaviors and heat transfer of a micropolar fluid over a permeable shrinking sheet taking into account the effect of thermal radiation. Hsiao [13] analyzed the flow behaviors of magnetohydrodynamic micropolar nanofluid flow towards a stretching sheet. He noted that the impact of magnetic field is pronounced at high temperature. As the polymer extrusion process occurs in a relatively high



temperature, there might be a considerable influence of the magnetic field.

The flow and heat transfer of natural convective flow along a vertical plate, which is kept in a porous medium, are investigated by Chamkha [14]. It was found that the skin friction and the heat transfer diminishes with higher values of Hartmann number and stratification number. On the other hand, Krishna and Chamkha [15] investigated the influences of Hall and ion slip on the nanofluid flow over a rotating vertical plate. Results showed a decrease in the heat transfer for increasing the suction and radiation absorption parameter. Yasin et al. [16] considered joule heating, viscous dissipation and velocity slip of an incompressible fluid over a stretching/shrinking sheet. Numerical solutions of similar equations expose that the magnetic parameter enhances the skin friction and heat transfer. Stagnation point flow over a stretching/shrinking cylinder was studied by Najib et al. [17] taking into account the chemical reaction. Dual solutions are identified for shrinking sheet but for stretching sheet only unique solutions exist.

The demand for heat transfer enhancement in numerous advanced technologies is growing day by day due to the reduction of size, but higher performance and storage capacities of the devices. In order to fulfil the needs, a new generation fluid called hybrid nanofluid has recently been introduced. It is well known that the heat transfer performance of hybrid nanofluids is better than that of nanofluids. A little attention is paid to the flow and heat transfer behaviors of hybrid nanofluids over a stretching/shrinking sheet. For example, Waini et al. [18, 19] studied the boundary layer flow and heat transfer over a nonlinear permeable stretching/shrinking sheet and an exponentially shrinking sheet, respectively. For Cu-Al<sub>2</sub>O<sub>3</sub>/water hybrid nanofluid, Devi and Devi [20] examined the heat transfer over a stretching sheet while Lund et al. [21] investigated the effects of viscous dissipation over a shrinking sheet. Shamshuddin et al. [22] assumed partial slip to examine the micropolar fluid flow over a stretching sheet. Recently, Al-Hanaya et al. [23] have examined the flow behavior and heat transfer of micropolar hybrid nanofluids over a stretching curved surface in the presence of magnetic field. Very good reviews on hybrid nanofluids are accomplished by Sarkar et al. [24], Sidik et al. [25], Sundar et al. [26], Babu et al. [27], Huminic and Huminic [28] and Sajid and Ali [29]. The interest in boundary layer flows and heat transfer due to a stretching/shrinking sheet is increasing substantially due to the large number of practical applications in industrial and manufacturing processes. Examples of such applications are drilling muds, plastic polymers, optical fibers, hot rolling paper production, metal spinning, cooling of metallic plates in cooling baths, manufacturing of polymer sheets, filaments and wires, etc. During the manufacturing process, the stretching/shrinking sheet is assumed to stretch/shrink on its own plane, and the stretched/shrinking surface interacts with the ambient fluid both mechanically and thermally. Stretching/shrinking can occur in a variety of materials each having a different strength, stretching transparency and lustre. Hybrid nanofluids are prepared either by dispersing dissimilar nanoparticles as individual constituents or by dispersing nanocomposite particles in the base fluid. These may possess better thermal network and rheological properties due to synergistic effect. Researchers, to adjudicate the advantages, disadvantages and their suitability for diversified applications, are extensively investigating the behavior and properties of these hybrid nanofluids. The estimation of heat transfer characteristics and pressure drop of the hybrid nanofluids are very important in order using these types of nanofluids in heat transfer applications. Thus, heat transfer characteristics and pressure drop of the hybrid nanofluids were investigated in some studies carried out. The review on hybrid nanofluid by Huminic and Huminic [22] revealed that hybrid nanofluids, with few exceptions, have thermal conductivities and viscosities higher than their base fluid and increase with increasing nanoparticles concentration. The factors which affect the thermo-physical properties of the hybrid nanoparticles are: the type of hybrid nanoparticles, the nanoparticles concentration, the base fluid, temperature, the time sonication, the addition or not of the surfactant as well as the mixing ratio of the two nanoparticles. Also, this review showed that hybrid nanofluids exhibit different rheological behaviors (Newtonian and non-Newtonian).

From the literature review, it is evident that no study has considered the unsteady boundary layer flow of a micropolar hybrid nanofluid over a stretching/shrinking sheet. The purpose of this study is to reveal the boundary layer separation criterion of micropolar hybrid nanofluid over a stretching/shrinking sheet considering the effect of magnetic field. The governing equations of the problem are reduced to a set of nonlinear differential equations using similarity transformations. Numerical results are demonstrated with local friction factor, local couple-stress and local Nusselt number as well as flow properties for different values of the pertinent parameters.

## 2. Problem Formulation

We assume an unsteady two-dimensional boundary layer flow of a micropolar hybrid nanofluid over a permeable stretching/shrinking sheet. We also presume that there exists a uniform magnetic field of strength  $B_0$  normal to the sheet. The schematic of the shrinking sheet and the coordinate system are shown in Fig. 1. The properties of the base fluid and the nanoparticles are considered to be constant. With the assumption of Boussinesq approximation, the governing equations of the problem are,

$$\frac{\partial \bar{u}}{\partial \bar{x}} + \frac{\partial \bar{v}}{\partial \bar{y}} = 0, \quad (1)$$

$$\frac{\partial \bar{u}}{\partial \bar{t}} + \bar{u} \frac{\partial \bar{u}}{\partial \bar{x}} + \bar{v} \frac{\partial \bar{u}}{\partial \bar{y}} = \frac{\partial \bar{u}_e}{\partial \bar{t}} + \bar{u}_e \frac{\partial \bar{u}_e}{\partial \bar{x}} + \frac{\mu_{hnf} + \kappa}{\rho_{hnf}} \frac{\partial^2 \bar{u}}{\partial \bar{y}^2} + \frac{\kappa}{\rho_{hnf}} \frac{\partial \bar{N}}{\partial \bar{y}} + \frac{g(\rho\beta)_{hnf}}{\rho_{hnf}} (\bar{T} - T_\infty) - \frac{\sigma_{hnf} B_0^2}{\rho_{hnf}} (\bar{u} - \bar{u}_e), \quad (2)$$

$$\frac{\partial \bar{N}}{\partial \bar{t}} + \bar{u} \frac{\partial \bar{N}}{\partial \bar{x}} + \bar{v} \frac{\partial \bar{N}}{\partial \bar{y}} = \frac{1}{\rho_{hnf}} \left( \mu_{hnf} + \frac{\kappa}{2} \right) \frac{\partial^2 \bar{N}}{\partial \bar{y}^2} - \frac{\kappa}{\rho_{hnf}} j \left( 2\bar{N} + \frac{\partial \bar{u}}{\partial \bar{y}} \right), \quad (3)$$

$$\frac{\partial \bar{T}}{\partial \bar{t}} + \bar{u} \frac{\partial \bar{T}}{\partial \bar{x}} + \bar{v} \frac{\partial \bar{T}}{\partial \bar{y}} = \alpha_{hnf} \frac{\partial^2 \bar{T}}{\partial \bar{y}^2}, \quad (4)$$

where  $\bar{x}$  and  $\bar{y}$  are the distances along and normal to the sheet,  $\bar{t}$  is the time,  $(\bar{u}, \bar{v})$  are the velocity components in the  $x$ - and  $y$ -directions,  $\bar{T}$  is the temperature of the fluid,  $\bar{N}$  is the component of microrotation in the  $\bar{x}\bar{y}$ -plane,  $\kappa$  is the vortex viscosity,  $j$  is the micro-inertia density and assumed to be constant,  $g$  is the acceleration due to gravity and  $\bar{u}_e$  is the local free stream velocity.



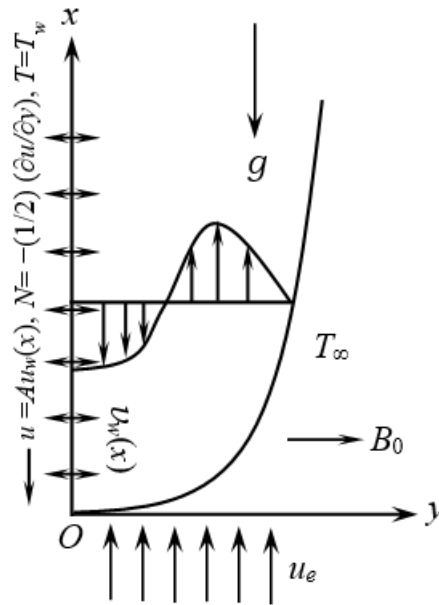


Fig. 1. Schematic of shrinking sheet and coordinate system

Moreover, the properties of the micropolar hybrid nanofluid such as the density  $\rho_{hnf}$ , the dynamic viscosity  $\mu_{hnf}$ , the thermal diffusivity  $\alpha_{hnf}$  and the electrical conductivity  $\sigma_{hnf}$  are given by

$$\begin{aligned}\mu_{hnf} &= \mu_f / (1 - \varphi_1 - \varphi_2)^{2.5}, \quad \rho_{hnf} = \varphi_1 \rho_1 + \varphi_2 \rho_2 + (1 - \varphi_{hnf}) \rho_f, \quad \varphi_{hnf} = \varphi_1 + \varphi_2, \\ \alpha_{hnf} &= \kappa_{hnf} / (\rho C)_{hnf}, \quad (\rho C)_{hnf} = \varphi_1 (\rho C)_1 + \varphi_2 (\rho C)_2 + (1 - \varphi_{hnf}) (\rho C)_f, \\ \frac{\kappa_{hnf}}{\kappa_f} &= \frac{(\varphi_1 \kappa_1 + \varphi_2 \kappa_2 + 2\kappa_f \varphi_{hnf}) - 2\varphi_{hnf} \{ \varphi_{hnf} \kappa_f - (\varphi_1 \kappa_1 + \varphi_2 \kappa_2) \}}{(\varphi_1 \kappa_1 + \varphi_2 \kappa_2 + 2\kappa_f \varphi_{hnf}) + \varphi_{hnf} \{ \kappa_f \varphi_{hnf} - (\varphi_1 \kappa_1 + \varphi_2 \kappa_2) \}}, \\ (\rho\beta)_{hnf} &= \varphi_1 (\rho\beta)_1 + \varphi_2 (\rho\beta)_2 + (1 - \varphi_{hnf}) (\rho\beta)_f, \\ \frac{\sigma_{hnf}}{\sigma_f} &= \frac{(\varphi_1 \sigma_1 + \varphi_2 \sigma_2 + 2\sigma_f \varphi_{hnf}) - 2\varphi_{hnf} \{ \varphi_{hnf} \sigma_f - (\varphi_1 \sigma_1 + \varphi_2 \sigma_2) \}}{(\varphi_1 \sigma_1 + \varphi_2 \sigma_2 + 2\sigma_f \varphi_{hnf}) + \varphi_{hnf} \{ \sigma_f \varphi_{hnf} - (\varphi_1 \sigma_1 + \varphi_2 \sigma_2) \}},\end{aligned}\quad (5)$$

where  $\kappa_{hnf}$  is the thermal conductivity of the micropolar hybrid nanofluid,  $\rho_f$ ,  $\mu_f$ ,  $\kappa_f$  and  $\sigma_f$  are the density, dynamic viscosity, thermal conductivity and electrical conductivity of the base fluid and  $(\rho C)_{hnf}$  is the effective heat capacity of the micropolar hybrid nanofluid and the subscripts  $f$ , 1, 2 represent the properties of the base fluid and two different types of nanoparticles.

The associated boundary conditions are

$$\bar{v} = v_w, \quad \bar{u} = u_w(\bar{x}, \bar{t}), \quad \bar{N} = -\frac{1}{2} \frac{\partial \bar{u}}{\partial \bar{y}}, \quad \bar{T} = T_w = T_\infty + \frac{T_0 \bar{x}}{(1 - b\bar{t})^2} \quad \text{at } \bar{y} = 0, \quad (6)$$

$$\bar{u} = \bar{u}_e(\bar{x}, \bar{t}), \quad \bar{N} = 0, \quad \bar{T} = T_\infty \quad \text{as } \bar{y} \rightarrow \infty. \quad (7)$$

where  $v_w$  is the rate of wall mass transfer,  $u_w(\bar{x}, \bar{t}) = c\bar{x} / (1 - b\bar{t})$  is the velocity of the sheet where  $c > 0$  is a constant and  $b$  measures the unsteadiness of the problem,  $T_0$  is a constant and  $\bar{u}_e(\bar{x}, \bar{t}) = a\bar{x} / (1 - b\bar{t})$  is the velocity outside the boundary layer.

If the kinematic viscosity of the pure fluid is  $\nu_f$ , then we define

$$\psi = \left( \frac{a\nu_f}{1 - b\bar{t}} \right)^{1/2} \bar{x} f(\eta), \quad \eta = y \left( \frac{a}{\nu_f(1 - b\bar{t})} \right)^{1/2}, \quad N = \nu_f^{-1/2} \left( \frac{a}{1 - b\bar{t}} \right)^{3/2} x g(\eta), \quad \theta(\eta) = \frac{\bar{T} - T_\infty}{T_w - T_\infty}, \quad (8)$$

with velocity components

$$u = \frac{\partial \psi}{\partial y}, \quad v = -\frac{\partial \psi}{\partial x}. \quad (9)$$

Thus the equations (2)-(4) reduce to

$$\frac{\mu_r}{\rho_r} \left( 1 + \frac{K}{\mu_r} \right) f''' + f f'' - f'^2 + 1 - \delta \left( f' + \frac{1}{2} \eta f'' - 1 \right) + \frac{K}{\rho_r} g' + \text{Ri} \frac{(\rho\beta)_r}{\rho_r} \theta - \frac{\sigma_r}{\rho_r} M (f' - 1) = 0, \quad (10)$$



$$\frac{\mu_r}{\rho_r} \left( 1 + \frac{K}{2\mu_r} \right) g'' + fg' - f'g - \frac{1}{2} \delta \eta g' - \frac{K}{\rho_r} B(2g + f'') = 0, \quad (11)$$

$$\frac{\alpha_r}{Pr} \theta'' + f\theta' - f'\theta - \frac{1}{2} \delta \eta \theta' = 0. \quad (12)$$

where  $K=\kappa/\mu_f$  is the vortex viscosity parameter,  $\delta=b/a$  is the unsteadiness parameter,  $Ri = g(\rho\beta)_f T_0/(a^2 \rho_f)$  is the Richardson's number,  $M=\sigma_f B_0^2/(a\rho_f)$  is the magnetic field parameter and  $B=v_f/(ja)$  is the microinertia parameter. Also, the ratios of the quantities are

$$\mu_r = \frac{\mu_{hnf}}{\mu_f}, \quad \rho_r = \frac{\rho_{hnf}}{\rho_f}, \quad (\rho C)_r = \frac{(\rho C)_{hnf}}{(\rho C)_f}, \quad (\rho\beta)_r = \frac{(\rho\beta)_{hnf}}{(\rho\beta)_f}, \quad \alpha_r = \frac{\alpha_{hnf}}{\alpha_f} \quad (13)$$

where  $\alpha_f$  is the thermal diffusivity of the fluid. The boundary conditions (6) become

$$f = s, f' = \gamma, g = -\frac{1}{2} f'', \theta = 1 \text{ at } \eta = 0, \quad (14)$$

$$f' = 1, g = 0, \theta = 0 \text{ as } \eta \rightarrow \infty. \quad (15)$$

In Eq. (14), the mass flux is assumed to be  $v_w(t) = -(av_f/(1-bt))^{1/2}s$  where  $s > 0$  or  $< 0$  is a suction or injection parameter and the constant  $\gamma=c/a$  is the velocity ratio parameter.

Here the interest is to reveal the characteristics of the local friction factor,  $C_f$ , local couple stress,  $m$ , and local Nusselt number,  $Nu$ , which are given by

$$C_f = \frac{1}{\rho_f u_e^2} \left[ \left( \mu_{hnf} + \kappa \right) \left( \frac{\partial \bar{u}}{\partial \bar{y}} \right) + \kappa \bar{N} \right]_{\bar{y}=0}, \quad m = \frac{\bar{\kappa}}{\rho_f u_e^2} \left( \mu_{hnf} + \frac{\kappa}{2} \right) \left( \frac{\partial \bar{N}}{\partial \bar{y}} \right)_{\bar{y}=0} \quad \text{and} \quad Nu = -\frac{\bar{\kappa} \kappa_{hnf}}{\kappa_f (T_w - T_\infty)} \left( \frac{\partial \bar{T}}{\partial \bar{y}} \right)_{\bar{y}=0}. \quad (16)$$

Combining (8), (9) and (16), we thus have

$$Re_x^{1/2} C_f = \left( \mu_r + \frac{K}{2} \right) \left( \frac{\partial^2 f}{\partial \eta^2} \right)_{\eta=0}, \quad m = \left( \mu_r + \frac{K}{2} \right) \left( \frac{\partial g}{\partial \eta} \right)_{\eta=0} \quad \text{and} \quad Re_x^{-1/2} Nu = -\frac{\kappa_{hnf}}{\kappa_f} \left( \frac{\partial \theta}{\partial \eta} \right)_{\eta=0}. \quad (17)$$

where  $Re_x = u_e x / \nu_f$  is the local Reynolds number.

### 3. Results and Discussion

The nonlinear ordinary differential equations (10)-(12) subject to boundary conditions (14) and (15) are solved using the implicit Runge-Kutta-Butcher method [30] with Nachtsheim-Swigert iteration scheme [31]. For the justification of the present solutions, a comparison is shown in Table 1. It is clear from the Table 1 that a good agreement exists between the present solutions and Lok et al. [7]. The physical properties used in this study are tabulated in Table 2.

**Table 1.** Comparison of  $f''(0)$  and  $\theta'(0)$  with boundary condition  $g(0)=0$  for  $Pr = 0.7$ ,  $\delta=0.0$ ,  $M=0.0$ ,  $S=0.0$ ,  $\varphi_1=0.0$  and  $\varphi_2=0.0$ .

K=0.0								
$f''(0)$					$-\theta'(0)$			
Lok et al. [7]		Present Method			Lok et al. [7]		Present Method	
Ri	Upper	Lower	Upper	Lower	Upper	Lower	Upper	Lower
-1.1	0.631500	-0.350112	0.631464	-0.350108	0.623645	-0.174184	0.623620	-0.174175
-1.4	0.440161	-0.494103	0.440161	-0.494123	0.590876	-0.044670	0.590876	-0.044373
-1.7	0.225110	-0.574153	0.225076	-0.574175	0.549039	0.073815	0.549016	0.073808
-2.0	-0.039513	-0.578523	-0.039513	-0.578473	0.486576	0.198572	0.486576	0.198600
K=3.0								
-1.1	0.338030	-	0.337999	-	0.541072	-	0.541068	-
-1.4	0.272370	-0.232634	0.272292	-0.232717	0.523074	-0.149524	0.523011	-0.149668
-1.7	0.202475	-0.273943	0.202365	-0.273948	0.502420	-0.059325	0.502337	-0.059338
-2.0	0.126644	-0.301711	0.126472	-0.301728	0.477863	0.020609	0.477734	0.020583

**Table 2.** Physical properties of base fluid and nanoparticles [15]

Physical Properties	Fluid (H <sub>2</sub> O)	Al <sub>2</sub> O <sub>3</sub>	Cu
$c_p$ (J/kgK)	4179	765	385
$\rho$ (kg/m <sup>3</sup> )	997.1	3970	8933
$\kappa$ (W/mK)	0.613	40	401
$\theta \times 10^{-5}$ (1/K)	21	0.85	1.67
$\sigma$ (N/m) <sup>-1</sup>	0.05	$3.69 \times 10^7$	$5.96 \times 10^7$



**Table 3.** Variations of local friction factor, local couple stress and local Nusselt number with  $\gamma$  when  $\phi_1=0.1$ ,  $\phi_2=0.05$ ,  $Pr = 6.2$ ,  $Ri=1.0$ ,  $M=1.0$ ,  $s=3.0$  and  $\delta=-2.0$ .

K=0.0						
$r$	$Re_x^{-1/2} C_f$		$m$		$Re_x^{-1/2} Nu$	
	Upper	Lower	Upper	Lower	Upper	Lower
0.0	5.887189	-24.071280	11.479570	91.307328	18.627254	17.004689
-0.5	8.507006	-21.193337	16.045048	57.563822	18.272340	16.457640
-1.0	10.9140389	-18.438870	19.844771	36.641435	17.898689	15.851655
-1.5	13.080316	-15.779701	22.835164	23.074064	17.503496	15.186106
-2.0	14.971618	-13.168670	24.966267	14.011448	17.082887	14.472034
-2.5	16.549833	-10.542728	26.179419	7.875797	16.629147	13.740753
-3.0	17.746954	-7.809514	26.375395	3.759259	16.133054	13.044250
-3.5	18.456309	-4.829102	25.403129	1.180649	15.579029	12.449889
-4.0	18.477444	-1.370872	22.97155	0.021527	14.933231	12.036884
-4.5	17.273949	3.144068	18.337869	0.752601	14.109988	11.920198
-4.91	11.885107	11.234627	8.255484	7.404497	12.738728	12.633757
K=1.0						
0.0	6.098423	-19.779120	9.149557	-20.838833	18.586354	17.675933
-0.5	8.746083	-16.904454	12.574603	-17.325329	18.211948	17.204960
-1.0	11.117402	-14.175469	15.233591	-14.399376	17.811600	16.690202
-1.5	13.166091	-11.539136	17.069887	-12.001089	17.384494	16.124902
-2.0	14.835933	-8.9111194	18.015280	-10.034155	16.923329	15.507464
-2.5	16.037109	-6.164667	17.961049	-8.349610	16.416848	14.853112
-3.0	16.609404	-3.082131	16.713746	-6.695466	15.844837	14.205903
-3.5	16.187462	0.745484	13.833492	-4.576946	15.161468	13.664983
-4.0	12.979791	7.165191	7.1712594	0.2189512	14.150522	13.510257
-4.07	10.513151	10.128600	3.788519	3.327092	13.777852	13.734498

**Table 4.** Variations of local friction factor, local couple stress and local Nusselt number with  $\gamma$  when  $\phi_1=0.1$ ,  $\phi_2=0.05$ ,  $Pr = 6.2$ ,  $Ri=1.0$ ,  $M=1.0$ ,  $K=1.0$  and  $\delta=-5.0$ .

s=1.0						
$r$	$Re_x^{-1/2} C_f$		$m$		$Re_x^{-1/2} Nu$	
	Upper	Lower	Upper	Lower	Upper	Lower
0.0	2.379920	-13.246967	2.080827	-10.524208	8.645749	7.113571
-0.5	2.271663	-9.582317	1.483410	-7.832201	7.900350	6.572769
-1.0	-1.137262	-3.035488	-1.990424	-3.440390	6.707228	6.465333
-1.01	-1.709640	-2.426263	-2.446957	-2.993703	6.617814	6.526553
s=2.0						
0.0	4.455871	-22.939644	5.888782	-23.683385	13.769999	12.260271
-0.5	5.924140	-19.065549	7.299080	-19.427252	13.258770	11.736350
-1.0	6.709566	-14.914455	7.528945	-15.360411	12.687488	11.226225
-1.5	6.410122	-10.066823	6.174736	-11.072761	12.016181	10.779716
-2.0	2.831191	-2.292596	0.997260	-4.303604	11.043359	10.617122
-2.04	1.434893	0.603842	0.579671	-2.685989	10.869019	10.698457
s=4.0						
0.0	8.574766	-54.861097	18.573356	-87.812714	24.852139	23.541240
-0.5	12.440106	-49.594901	26.312224	-77.848541	24.544378	23.199928
-1.0	16.010496	-44.383954	33.007405	-68.495874	24.225513	22.849738
-1.5	19.254753	-39.195891	38.605702	-59.703484	23.893977	22.491290
-2.0	22.132088	-33.986163	43.037601	-51.400418	23.547764	22.125876
-2.5	24.587152	-28.693108	46.208950	-43.487608	23.184185	21.755799
-3.0	26.540609	-23.228355	47.985055	-35.821547	22.799449	21.384946
-3.5	27.869621	-17.457236	48.157744	-28.181055	22.387824	21.019818
-4.0	28.360244	-11.151288	46.365090	-20.186886	21.939627	20.671723
-4.5	27.555172	-3.836315	41.834737	-11.045246	21.435003	20.363197
-5.0	23.853160	6.106649	31.866144	1.967756	20.808396	20.163623
-5.21	16.894912	15.614807	18.407851	16.251058	20.335105	20.287378

The influences of the vortex viscosity parameter,  $K$ , on the local friction factor,  $Re_x^{-1/2}C_f$ , local couple-stress,  $m$ , and local Nusselt number,  $Re_x^{-1/2}Nu$ , are shown in Figs. 2(a)-(c), respectively. Also, the numerical values of the above quantities are presented in Table 3 considering different values of  $K$ . It is evident from the figures and Table 3 that for increasing the magnitude of the velocity ratio parameter, the local friction factor and the local couple-stress corresponding to stable solutions first increase and then decrease until the occurrence of the critical points. On the other hand, the local Nusselt number gradually decreases with  $\gamma$ . The unstable solutions for  $K=0.0$ ,  $0.05$ ,  $0.1$  and  $0.25$  show a distinct pattern from those for  $K=0.5$  and  $1.0$ . Results indicate that the vortex viscosity parameter reduces the local friction factor, local couple-stress and local Nusselt number. In Fig. 2(d), the variations of the critical values of the velocity ratio parameter,  $\gamma_c$ , local friction factor,  $Re_x^{-1/2}C_{f,c}$ , local couple-stress,  $m_c$ , and local Nusselt number,  $Re_x^{-1/2}Nu_c$ , with the change of  $K$  are illustrated. Due to the increase of the vortex viscosity parameter, the magnitude of the critical point exponentially diminishes. So, the boundary layer separation accelerates for higher values of  $K$ . Moreover, for higher values of  $K$  the critical value of the local Nusselt number exponentially increases, but that of the local friction factor and couple-stress is found to decrease exponentially. The dependency of the critical values of velocity ratio parameter, local friction factor, local



couple-stress and local Nusselt number on the value of  $K$  ( $0 \leq K \leq 10$ ) can be represented in the following functions:

$$\gamma_c(K) = -2.96944 + 0.189675K + 0.003867571e^{0.945948K} - 1.48287e^{-0.82205K} - 0.0116525KF\left(\frac{1}{2}, 2, K\right),$$

$$\text{Re}_x^{1/2} C_{fc}(K) = -21.3031 - 3.04251K + 28.6676e^{-0.0582121K} - 0.00334501KF\left(\frac{1}{4}, 3, K\right),$$

$$m_c(K) = -7.26553 - 0.118928K + 16.1955e^{-0.368651K} - 0.00105029KF\left(\frac{1}{4}, 3, K\right),$$

$$\text{Re}_x^{-1/2} \text{Nu}_c(K) = 16.2281 + 0.120345K - 1.9684e^{-0.756561K} - 0.000543922KF\left(\frac{1}{4}, 3, K\right),$$

where  $F(a, b, x)$  is the confluent hypergeometric function and is defined by

$$F(a, b, x) = \sum_{r=0}^{\infty} \frac{(a)_r}{(b)_r} \frac{x^r}{r!},$$

where  $(a)_0=1$ ,  $(a)_r=a(a+1)(a+2)\dots(a+r-1)$ .

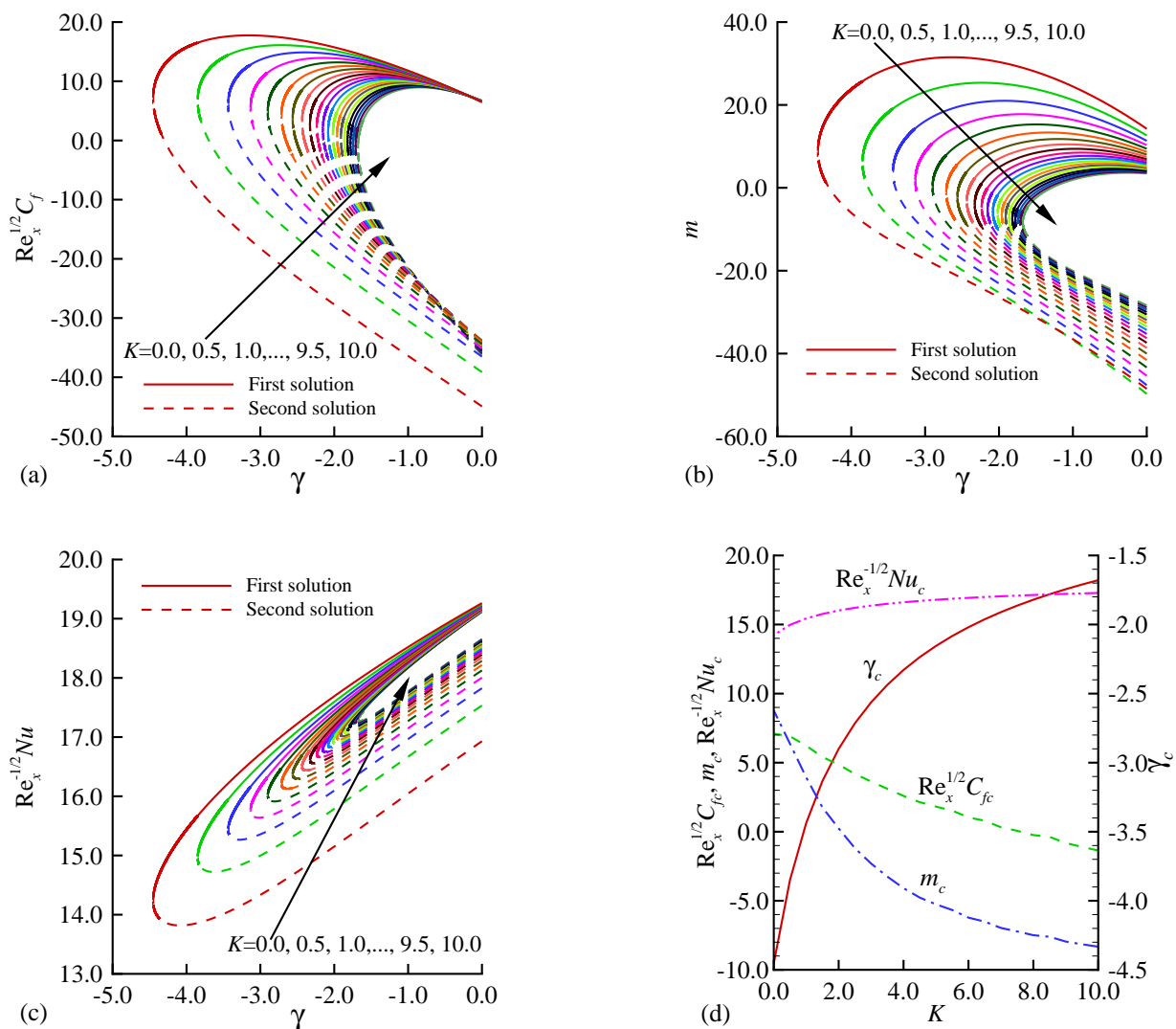


**Fig. 2.** (a) Local skin friction coefficient (b) local couple-stress, (c) local Nusselt number and (d) corresponding critical values for varying  $K$  when  $\varphi_1=0.1$ ,  $\varphi_2=0.05$ ,  $\text{Pr} = 6.2$ ,  $\text{Ri}=1.0$ ,  $M=1.0$ ,  $s=3.0$  and  $\delta=-5.0$ .

Figures 3(a)-(c) depict the variations of the local friction factor,  $\text{Re}_x^{1/2} C_f$ , local couple-stress,  $m$ , and local Nusselt number,  $\text{Re}_x^{-1/2} \text{Nu}$ , with the change of the suction parameter,  $s$ . These quantities are also tabulated in Table 4 for  $s=1.0$ ,  $2.0$  and  $4.0$ . From the figures and Table 4, it is seen that increasing values of  $s$  lead to significant increase in the local friction factor, local couple-stress and local Nusselt number. The effect of the suction parameter on the critical velocity ratio parameter,  $\gamma_c$ , and critical values of the local friction factor,  $\text{Re}_x^{1/2} C_{fc}$ , local couple-stress,  $m_c$ , and local Nusselt number,  $\text{Re}_x^{-1/2} \text{Nu}_c$ , is depicted in Fig. 3(d). It is found from Fig. 3(d) that all of the above quantities exponentially increase for increasing values of  $s$ . In this regard, the domain of the existence of dual solutions becomes wider for higher values of  $s$ . The critical values of the velocity ratio parameter,  $\gamma_c$ , local friction factor,





$Re_x^{-1/2}C_{fc}$ , local couple-stress,  $m_c$ , and local Nusselt number,  $Re_x^{-1/2}Nu_c$ , can be represented as a function of  $s$  ( $1 \leq s \leq 4$ ) as follows:

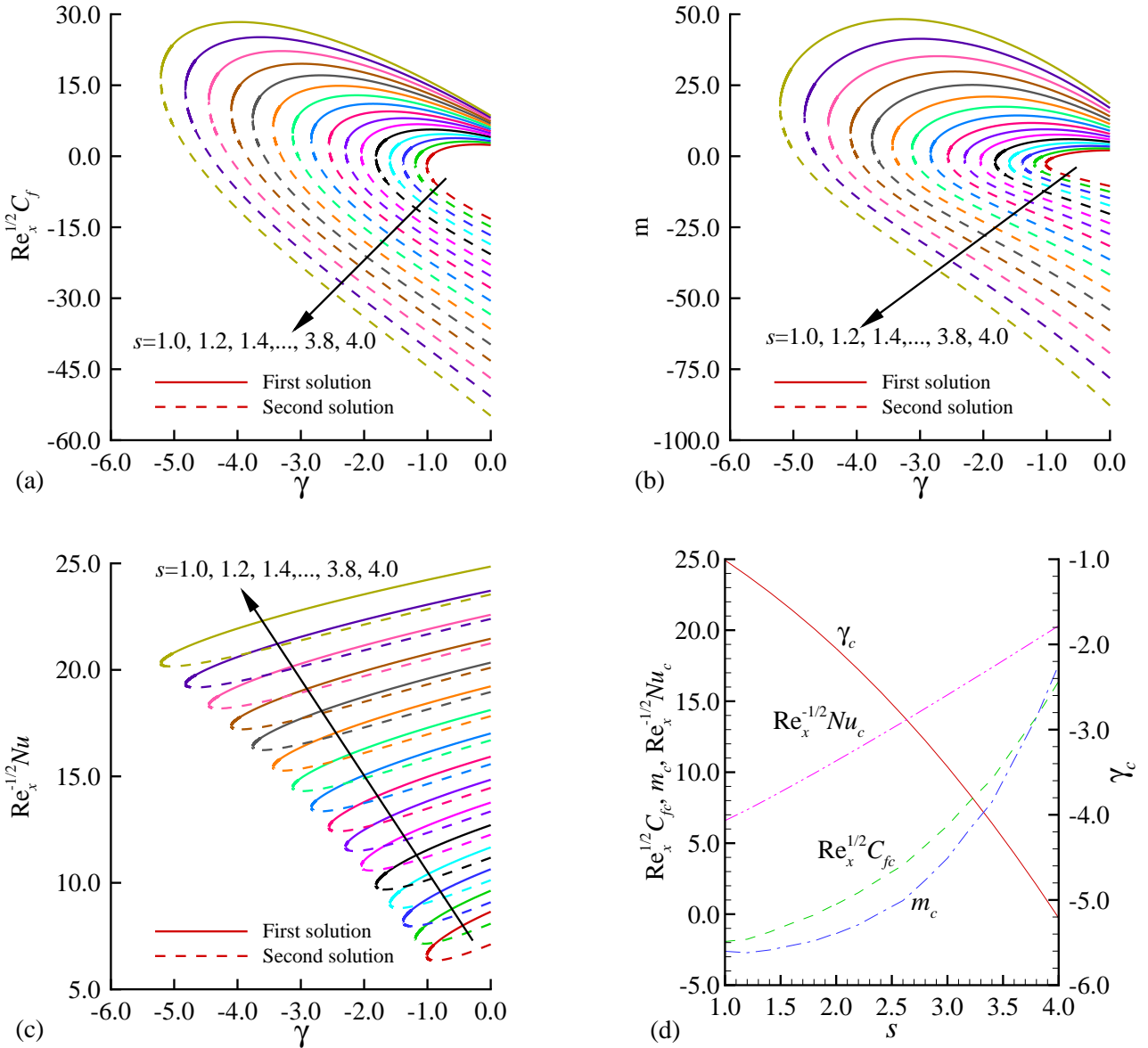


**Fig. 3.** (a) Local skin friction coefficient (b) local couple-stress, (c) local Nusselt number and (d) corresponding critical values for varying  $s$  when  $\phi_1=0.1$ ,  $\phi_2=0.05$ ,  $Pr = 6.2$ ,  $K=0.5$ ,  $Ri=1.0$ ,  $M=1.0$  and  $\delta=-5.0$ .

$$\gamma_c(s) = 1.82967 - 2.07364e^{0.315258s} - 284.896e^{-324.037s} + 0.000856974sF\left(\frac{1}{3}, \frac{1}{4}, s\right),$$

$$Re_x^{1/2}C_{fc}(s) = -4.24416 + 0.940961e^{0.930447s} - 21.4871e^{-44.2625s} - 0.0561681F\left(\frac{1}{3}, \frac{1}{4}, s\right),$$

$$m_c(s) = -6.54339 + 4.52055e^{0.69832s} + 30.112e^{-104.325s} - 4.33188F\left(\frac{1}{2}, 3, s\right),$$

$$Re_x^{-1/2}Nu_c(s) = 1.82594 + 3.44542s + 0.750075e^{1.14274s} + 371.775e^{-8.56319s} - 0.497495sF\left(\frac{1}{2}, \frac{2}{3}, s\right).$$

The effects of the magnetic field parameter,  $M$ , on the local friction factor,  $Re_x^{1/2}C_f$ , local couple-stress,  $m$ , and local Nusselt number,  $Re_x^{-1/2}Nu$ , are illustrated in Figs. 4(a)-(c), respectively. Due to the increase of the value of  $M$  there is seen a considerable increase in the local friction factor, local couple-stress and local Nusselt number. Figure 4(d) exhibits the influence of the magnetic field parameter on the critical values of the velocity ratio parameter,  $\gamma_c$ , local friction factor,  $Re_x^{1/2}C_{fc}$ , local couple-stress,  $m_c$ , and local Nusselt number,  $Re_x^{-1/2}Nu_c$ . A linear relation is observed between the critical value of the velocity ratio parameter and the magnetic field parameter and its gradient is positive. So, the boundary layer separation delays with the increase of the magnetic field parameter. With the increase of  $M$ , the value of  $Re_x^{1/2}C_{fc}$  increases, but the value of  $Re_x^{-1/2}Nu_c$  decreases. Contrary to this, when the value of  $M$  is increased from 0 to 4.5 the value of  $Re_x^{-1/2}Nu_c$  first increases and then decreases. From the numerical solutions, the relations between the value of  $M$  ( $0 \leq M \leq 4.5$ ) and the values of  $\gamma_c$ ,  $Re_x^{1/2}C_{fc}$ ,  $m_c$  and  $Re_x^{-1/2}Nu_c$  can be formulated as follows:



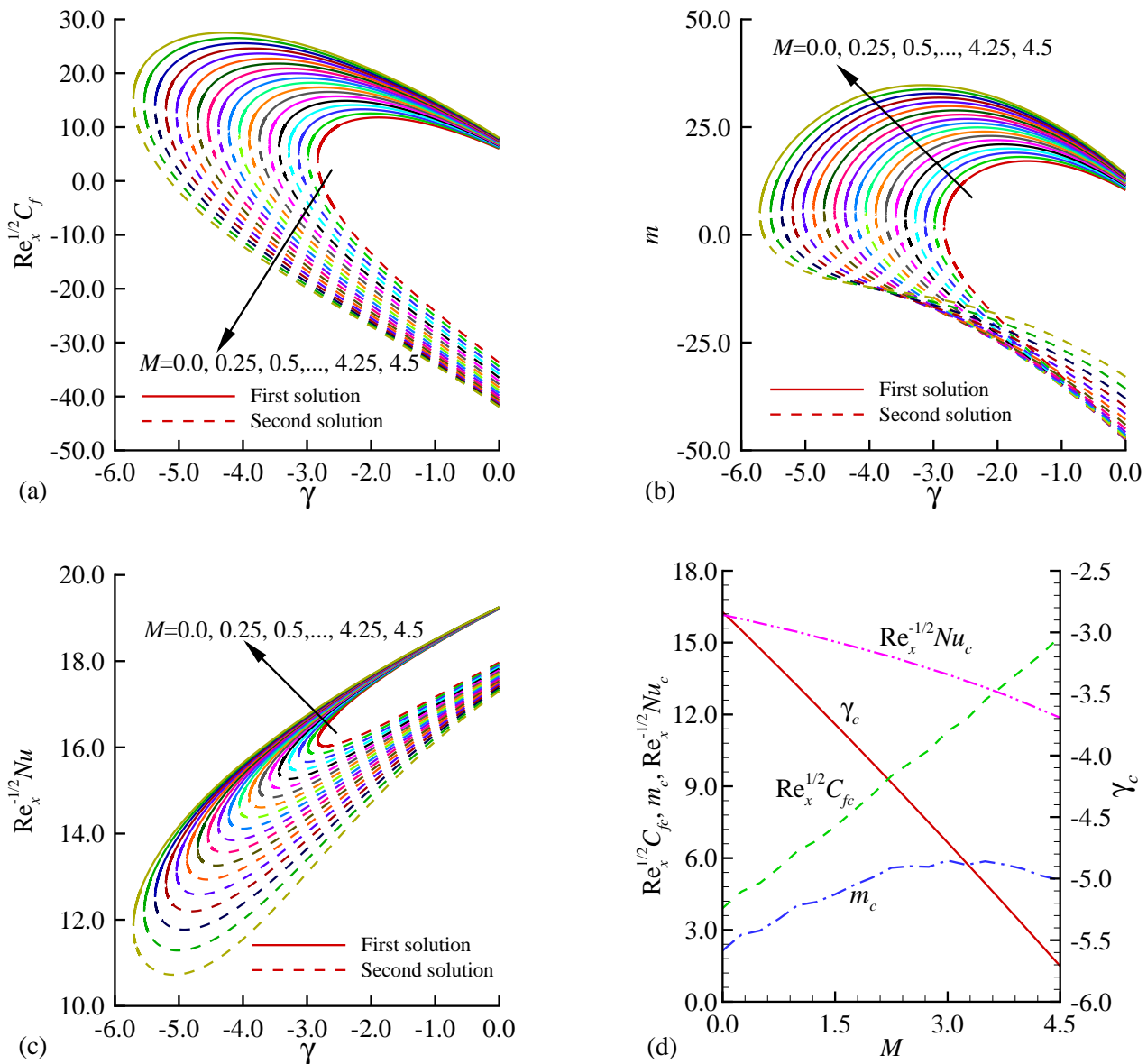


**Fig. 4.** (a) Local skin friction coefficient (b) local couple-stress, (c) local Nusselt number and (d) corresponding critical values for varying  $M$  when  $\phi_1=0.1$ ,  $\phi_2=0.05$ ,  $Pr = 6.2$ ,  $K=0.5$ ,  $Ri=1.0$ ,  $s=3.0$  and  $\delta=-5.0$ .

$$\gamma_c(M) = 12.1124 - 14.9469e^{0.0399376M} + 0.00601735MF\left(\frac{1}{3}, 3, M\right),$$

$$Re_x^{1/2} C_{fc}(M) = 3.2457 + 2.60386M + 0.711813e^{-0.834095M} + 0.0283508MF\left(\frac{1}{4}, 3, M\right),$$

$$m_c(M) = 2.76891 + 1.94912M - 0.544089e^{-1.01268M} + 0.406122M\left(\frac{1}{2}, 1, M\right),$$

$$Re_x^{-1/2} Nu_c(M) = 21.0548 - 4.89777e^{0.117223M} - 0.0979341MF\left(\frac{1}{4}, 3, M\right).$$

The variations of the local friction factor,  $Re_x^{1/2} C_f$ , local couple-stress,  $m$ , and local Nusselt number,  $Re_x^{-1/2} Nu$ , with the Richardson's number,  $Ri$ , is demonstrated in Figs. 5(a)-(c), respectively. The local friction factor, local couple-stress and local Nusselt number are found to increase for higher values of  $M$ . The critical points corresponding to  $M=0.0$ ,  $0.5$  and  $1.0$  are  $-3.66475$ ,  $-4.03850$ ,  $-4.41725$ , respectively. So, these results indicate that the dual solutions exist in broader region for larger values of  $M$ .

The effects of the volume fraction of Cu nanoparticles,  $\phi_2$ , on the local friction factor,  $Re_x^{1/2} C_f$ , local couple-stress,  $m$ , and local Nusselt number,  $Re_x^{-1/2} Nu$ , are shown in Figs. 6(a)-(c), respectively. The value of  $\phi_2$  considerably enhances the local friction factor and the local couple-stress, but causes a reduction in the local Nusselt number. Figure 5(d) demonstrates the critical values of the velocity ratio parameter,  $\gamma_c$ , local friction factor,  $Re_x^{1/2} C_{fc}$ , local couple-stress,  $m_c$ , and local Nusselt number,  $Re_x^{-1/2} Nu_c$ , with the change of  $\phi_2$ . It is thus evident from this figure that the domain of the existence of dual solutions exponentially increases owing to the increase of  $\phi_2$ . However, there is almost a linear relation between the value of  $\phi_2$  and the critical values of the local friction factor, local couple-stress and local Nusselt number. The changes of the critical values of the velocity ratio parameter, local friction factor, local couple-stress and local Nusselt number against  $\phi_2$  ( $0 \leq \phi_2 \leq 0.2$ ) can be written in the following relations:





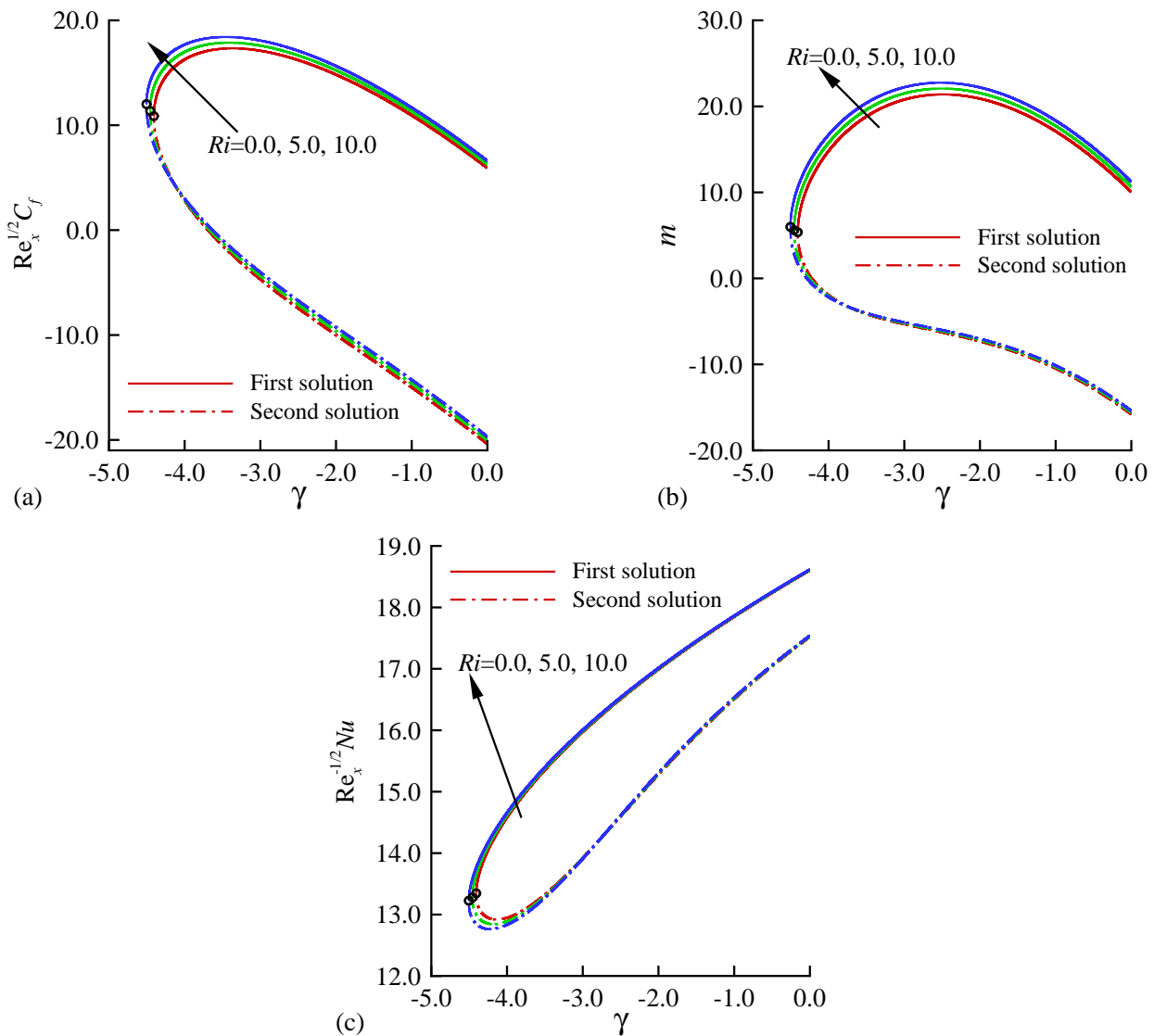


**Fig. 5.** (a) Local skin friction coefficient (b) local couple-stress, (c) local Nusselt number and (d) corresponding critical values for varying  $K$  when  $\varphi_1=0.1$ ,  $\varphi_2=0.05$ ,  $Pr = 6.2$ ,  $K = 0.5$ ,  $M=1.0$ ,  $s=3.0$  and  $\delta=-5.0$ .

$$\begin{aligned}\gamma_c(\varphi_2) &= -4.61373 + 1.66348e^{5.86097\varphi_2} + 2.45882\varphi_2 F\left(\frac{1}{3}, 3, \varphi_2\right), \\ \text{Re}_x^{-1/2} C_{fc}(\varphi_2) &= 9.48539 - 6.63926e^{-3.96862\varphi_2} + 10.864\varphi_2 F\left(\frac{1}{4}, \frac{1}{3}, \varphi_2\right), \\ m_c(\varphi_2) &= 0.209437 - 0.0640663e^{16.1808\varphi_2} + 37.1672\varphi_2 \left(\frac{1}{3}, \frac{1}{2}, \varphi_2\right), \\ \text{Re}_x^{-1/2} Nu_c(\varphi_2) &= 16.2345 + 0.477151e^{-15.696\varphi_2} - 8.9378\varphi_2 F\left(\frac{1}{4}, 3, \varphi_2\right).\end{aligned}$$

The influences of the unsteadiness parameter,  $\delta$ , on the local friction factor,  $\text{Re}_x^{-1/2} C_f$ , local couple-stress,  $m$ , and local Nusselt number,  $\text{Re}_x^{-1/2} Nu$ , are presented in Figs. 7(a)-(c), respectively. As the magnitude of  $\delta$  increases the local friction factor and the local couple-stress are found to decrease whereas the local Nusselt number increases. The changes of the critical values of the velocity ratio parameter,  $\gamma_c$ , local friction factor,  $\text{Re}_x^{-1/2} C_{fc}$ , local couple-stress,  $m_c$ , and local Nusselt number,  $\text{Re}_x^{-1/2} Nu_c$ , with the unsteadiness parameter are shown in Fig. 7(d). For increasing the magnitude of  $\delta$ , there is an increase in  $\text{Re}_x^{-1/2} C_{fc}$ ,  $m_c$  and the magnitude of  $\gamma_c$  but a decrease in  $\text{Re}_x^{-1/2} Nu_c$ . This tendency implies that the increase in the magnitude of  $\delta$  expedites the separation of the boundary layer. The values of  $\gamma_c$ ,  $\text{Re}_x^{-1/2} C_{fc}$ ,  $m_c$  and  $\text{Re}_x^{-1/2} Nu_c$  against the value of  $\delta$  can be stated as follows:

$$\begin{aligned}\gamma_c(\delta) &= -5.34565 - 0.064021e^{-0.137467\delta} - 0.855502\delta F\left(\frac{1}{2}, 2, \delta\right), \\ \text{Re}_x^{-1/2} C_{fc}(\delta) &= -30.561751.62e^{0.0364713\delta} + 7.17969\delta F\left(\frac{1}{4}, \frac{1}{3}, \delta\right), \\ m_c(\delta) &= -18.3462 + 6.15437 + 193.497e^{1.02622\delta} + 52.4787\delta \left(\frac{1}{2}, \frac{1}{3}, \delta\right), \\ \text{Re}_x^{-1/2} Nu_c(\delta) &= 2.62435 + 0.778484\delta + 0.00285618e^{-0.393045\delta} - 12.3622\delta F\left(\frac{1}{2}, 1, \delta\right).\end{aligned}$$



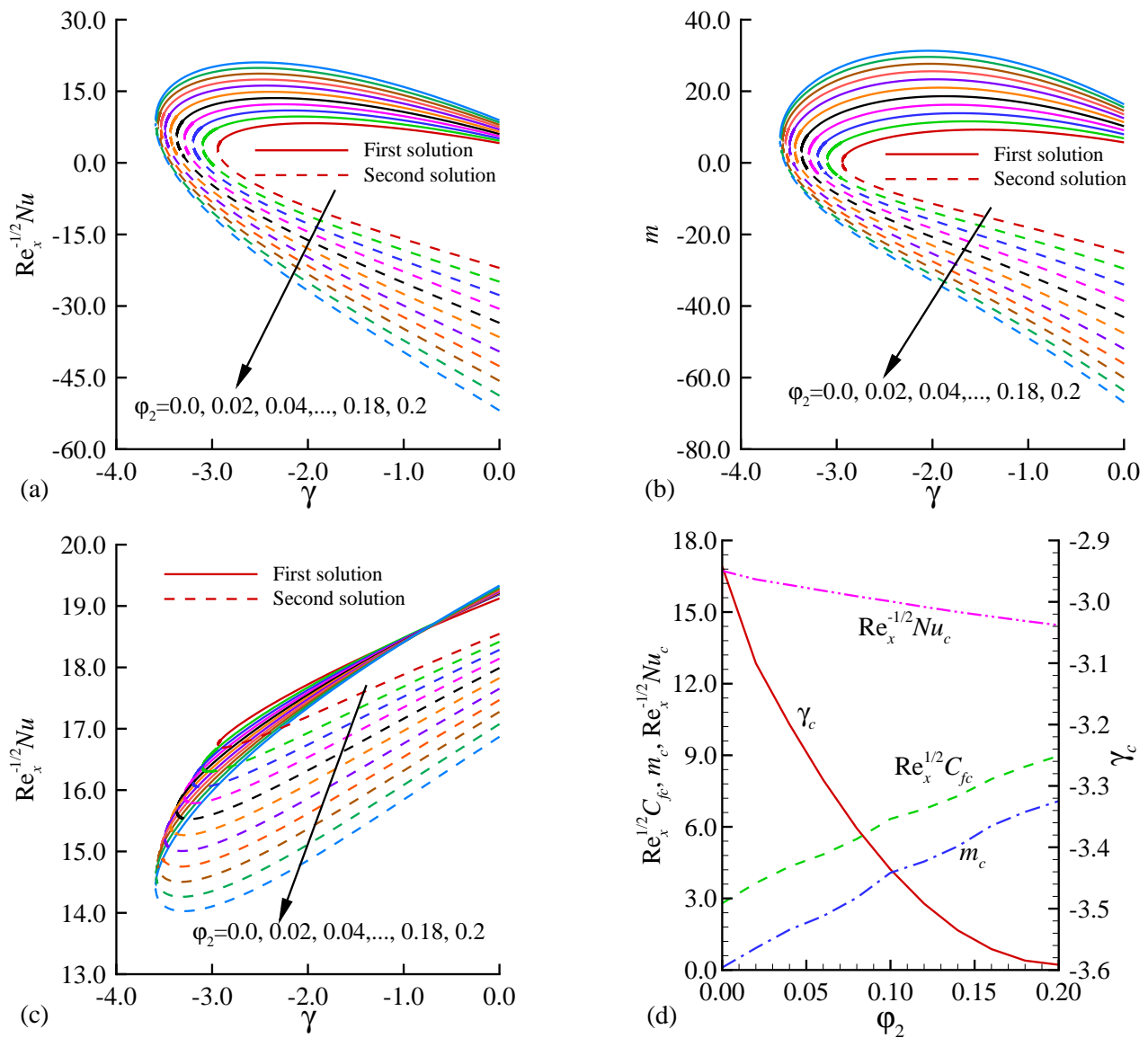


**Fig. 6.** (a) Local skin friction coefficient (b) local couple-stress , (c) local Nusselt number and (d) corresponding critical values for varying K when  $\phi_1=0.1$ ,  $Pr = 6.2$ ,  $K = 0.5$ ,  $Ri=1.0$ ,  $M=1.0$ ,  $s=3.0$  and  $\delta=-5.0$ .

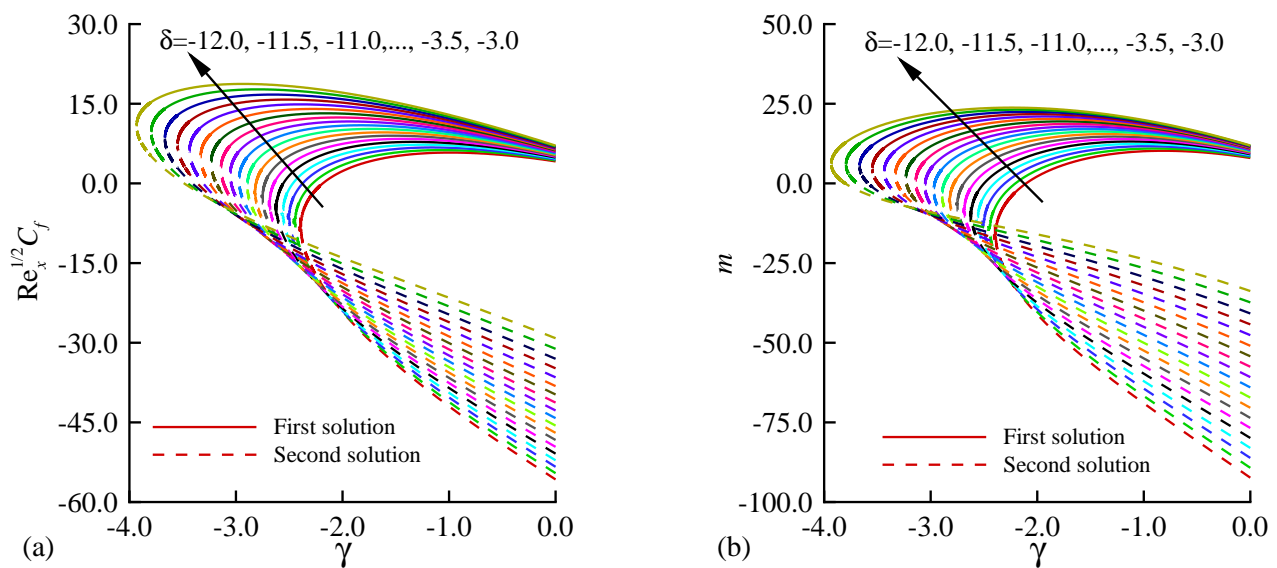


**Fig. 7.** (a) Local skin friction coefficient (b) local couple-stress , (c) local Nusselt number and (d) corresponding critical values for varying K when  $\phi_1=0.1$ ,  $\phi_2=0.05$ ,  $Pr = 6.2$ ,  $K = 0.5$ ,  $Ri=1.0$ ,  $M=1.0$  and  $s=3.0$ .



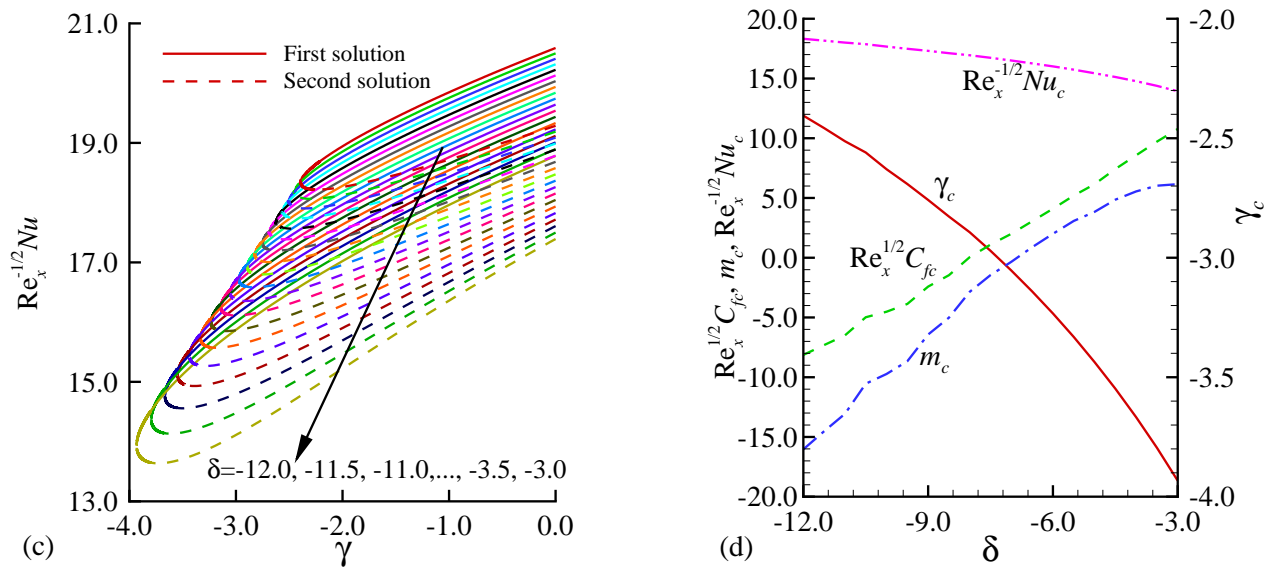


**Fig. 7.** (a) Local skin friction coefficient (b) local couple-stress, (c) local Nusselt number and (d) corresponding critical values for varying  $K$  when  $\varphi_1=0.1$ ,  $\varphi_2=0.05$ ,  $Pr = 6.2$ ,  $K = 0.5$ ,  $Ri=1.0$ ,  $M=1.0$  and  $s=3.0$ .

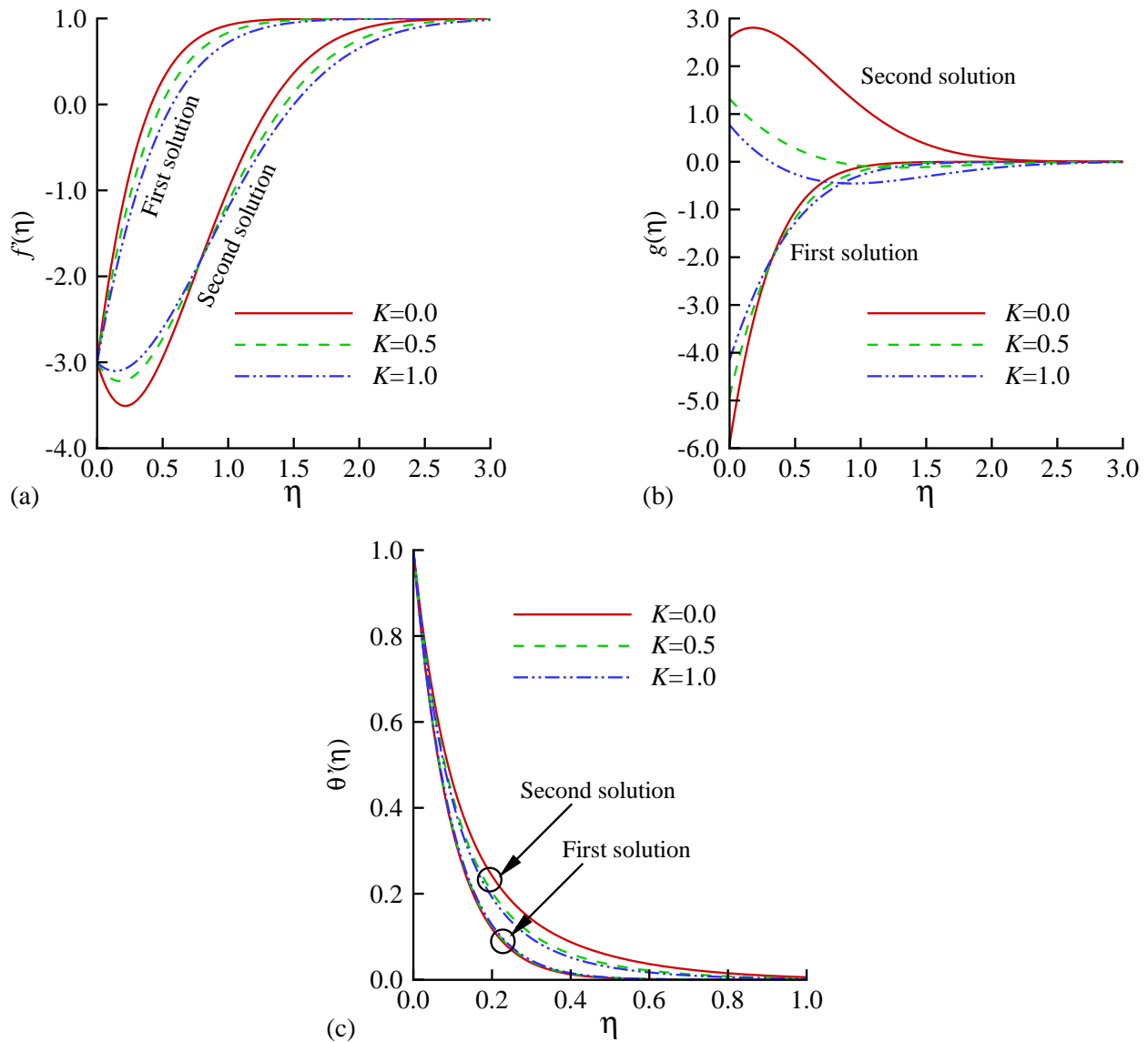


**Fig. 8.** (a) Velocity (b) angular velocity and (c) temperature for varying  $K$  when  $\varphi_1=0.1$ ,  $\varphi_2=0.05$ ,  $Pr = 6.2$ ,  $Ri=1.0$ ,  $M=1.0$ ,  $s=3.0$  and  $\delta=-2.0$ .



The velocity, angular velocity and temperature profiles for different values of  $K$  are shown in Figs. 8(a)-(c), respectively. Results show that an increase in the value of  $K$  diminishes the velocity, angular velocity and temperature. The momentum and thermal boundary layers increase a bit for higher values of  $K$ .

Figures 9(a)-(c) demonstrate the variations of the velocity, angular velocity and temperature for the change of the magnetic field parameter,  $M$ . Because of the increase of the value of  $M$  it is observed from the first solutions that the velocity of the fluid significantly increases, however, there is negligible impact on the angular velocity and temperature. In the case of second solutions, when the value of  $M$  is increased the velocity decreases, but the angular velocity and temperature are found to increase.

The influences of the Richardson's number,  $Ri$ , on the velocity, angular velocity and temperature are illustrated in Figs. 10(a)-(c), respectively. From the figures, it is clear that there is a very small effect of  $Ri$  on the velocity, angular velocity and temperature.

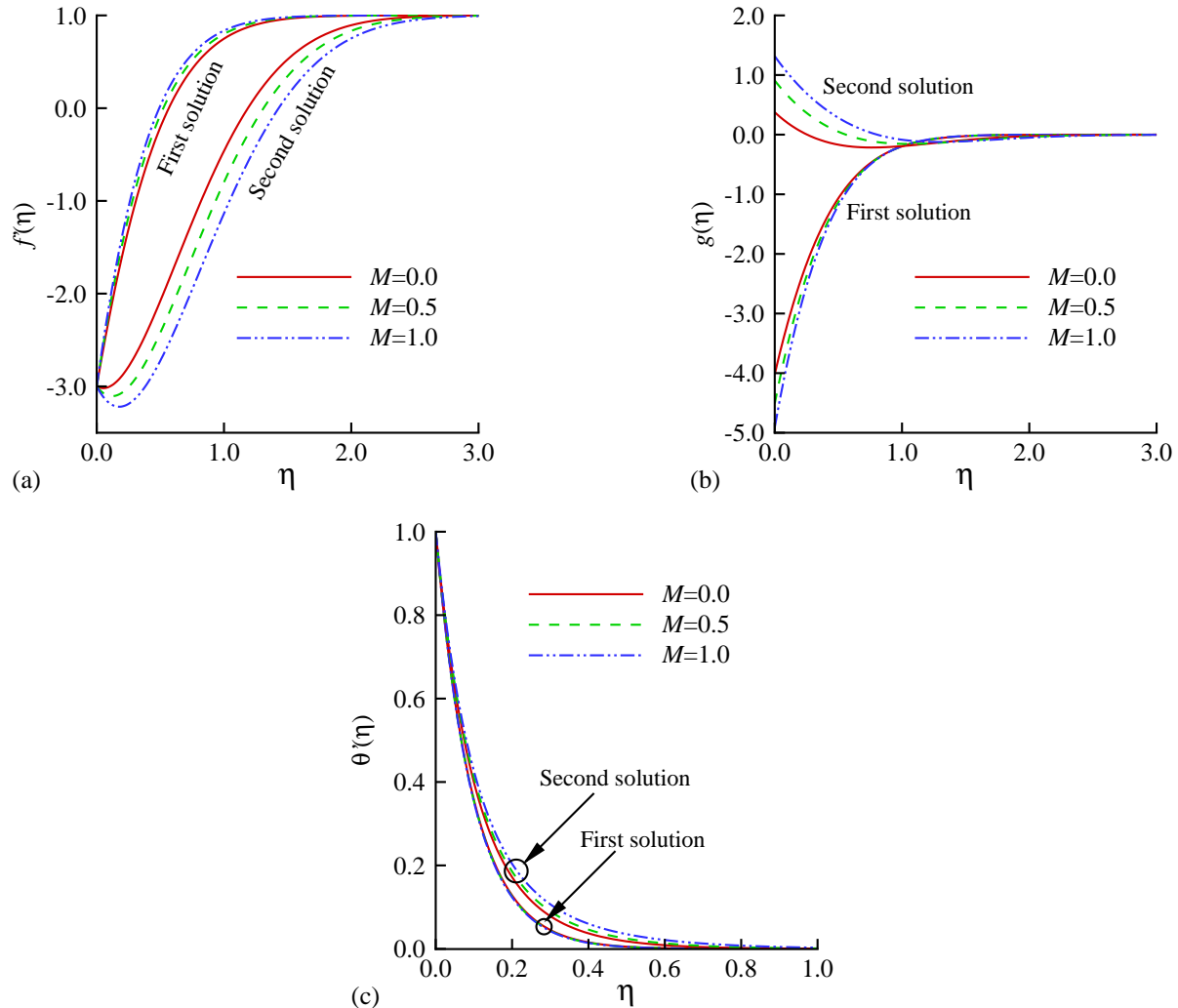


**Fig. 9.** (a) Velocity (b) angular velocity and (c) temperature for varying  $M$  when  $\varphi_1=0.1$ ,  $\varphi_2=0.05$ ,  $Pr = 6.2$ ,  $Ri=1.0$ ,  $K=0.5$ ,  $s=3.0$  and  $\delta=-2.0$ .

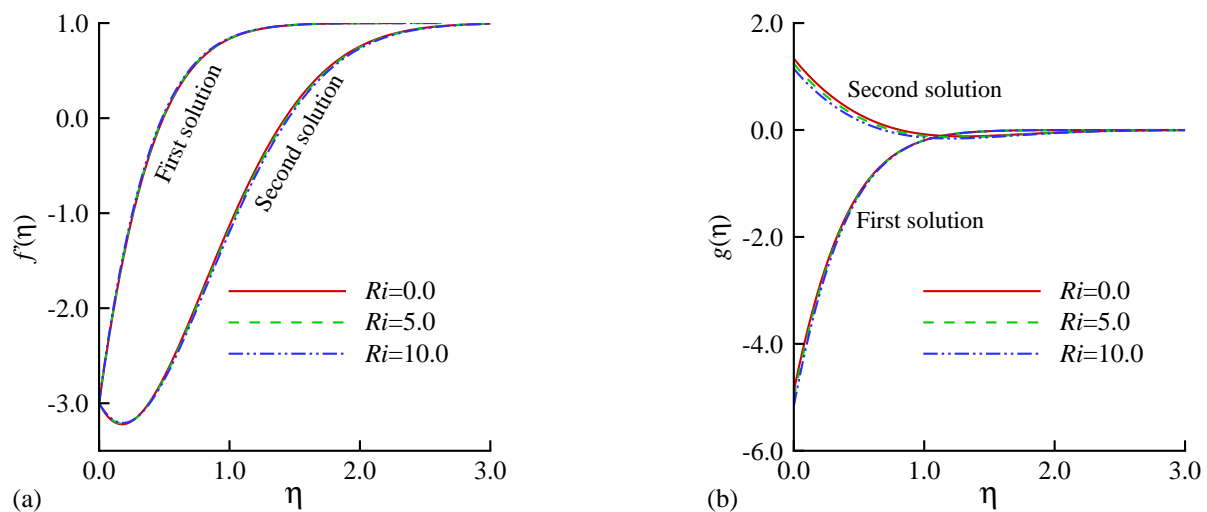


**Fig. 10.** (a) Velocity (b) angular velocity and (c) temperature for varying  $Ri$  when  $\varphi_1=0.1$ ,  $\varphi_2=0.05$ ,  $Pr = 6.2$ ,  $K=0.5$ ,  $M=1.0$ ,  $s=3.0$  and  $\delta=-2.0$ .



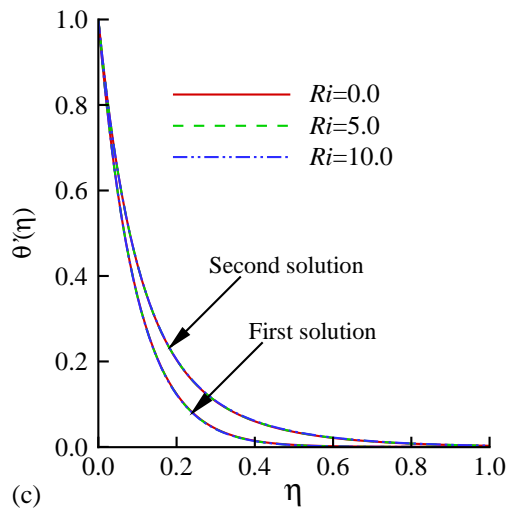


**Fig. 10.** (a) Velocity (b) angular velocity and (c) temperature for varying  $Ri$  when  $\phi_1=0.1$ ,  $\phi_2=0.05$ ,  $Pr = 6.2$ ,  $K=0.5$ ,  $M=1.0$ ,  $s=3.0$  and  $\delta=-2.0$ .

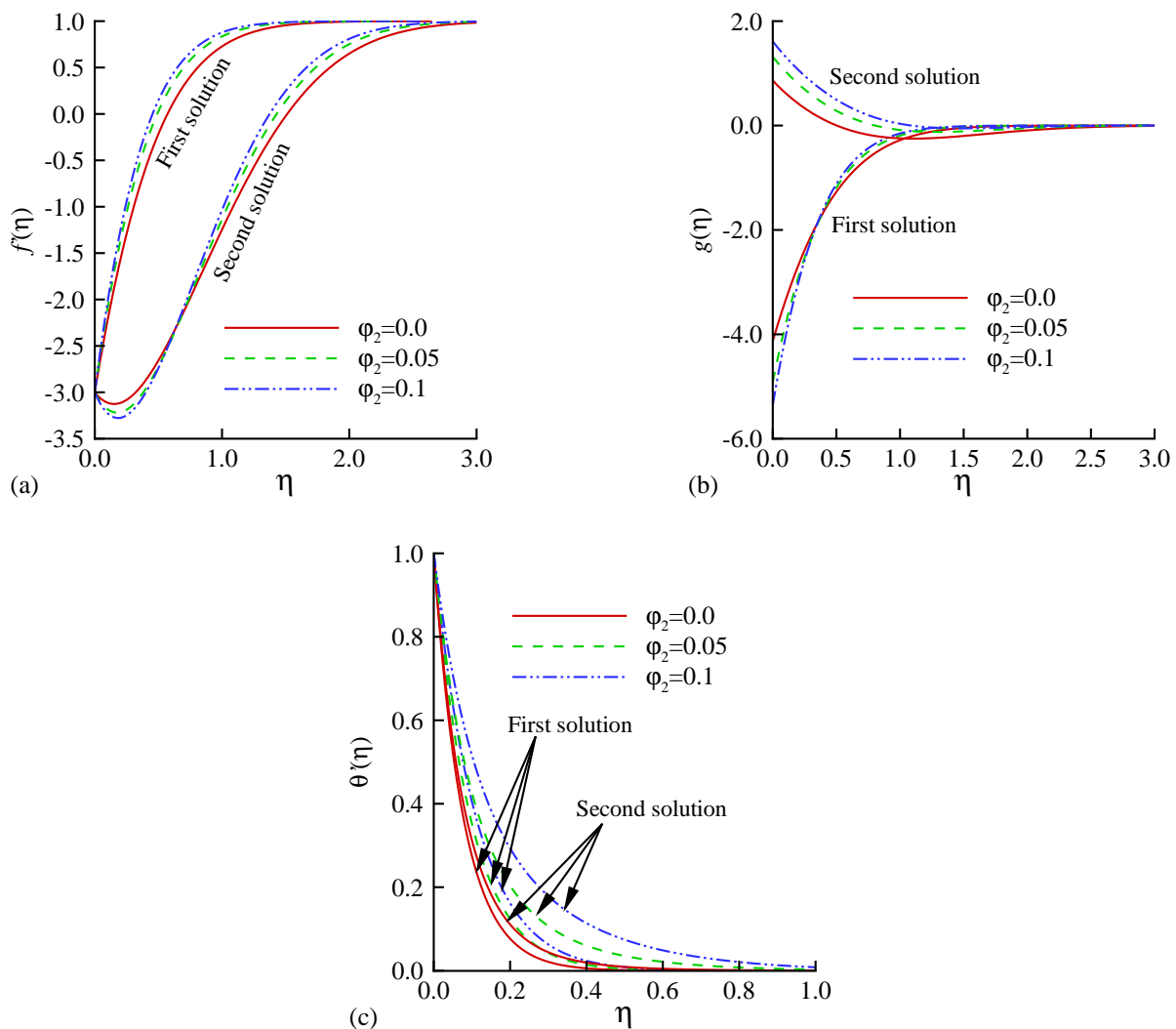


**Fig. 11.** (a) Velocity (b) angular velocity and (c) temperature for varying  $Ri$  when  $\phi_1=0.1$ ,  $Pr = 6.2$ ,  $Ri=1.0$ ,  $K=0.5$ ,  $M=1.0$ ,  $s=3.0$  and  $\delta=-2.0$ .

Figures 11(a)-(c) exhibit the influences of the volume fraction of Cu nanoparticles,  $\phi_2$ , on the velocity, angular velocity and temperature. It is seen that the velocity, angular velocity and temperature increase with the increase of  $\phi_2$ . The second solutions also show the similar tendency. It is also evident from the results that the momentum boundary layer decreases and the thermal boundary layer increases.

The effects of the suction parameter,  $s$ , on the velocity, angular velocity and temperature are elucidated in Figs. 12(a)-(c), respectively. For increasing the value of  $s$  the velocity and angular velocity increase, but the temperature decreases. Accordingly, the suction parameter reduces the momentum and thermal boundary layers.



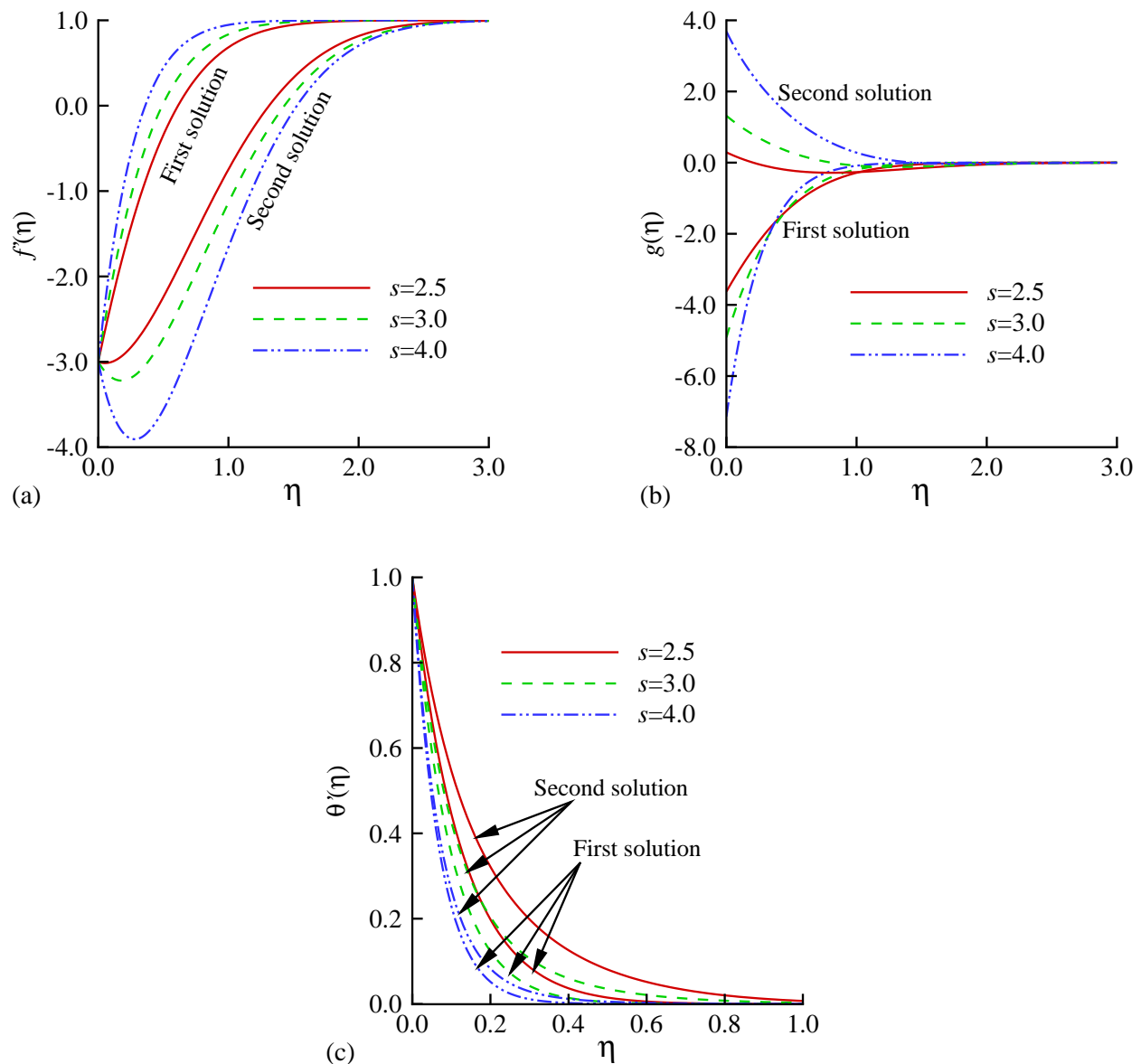


**Fig. 12.** (a) Velocity (b) angular velocity and (c) temperature for varying  $s$  when  $\varphi_1=0.1$ ,  $\varphi_2=0.05$ ,  $Pr = 6.2$ ,  $Ri=1.0$ ,  $K=0.5$ ,  $M=1.0$  and  $\delta=-2.0$ .

#### 4. Conclusion

In this study, the flow and heat transfer characteristics of a micropolar hybrid nanofluid over a non-isothermal stretching/shrinking sheet have been investigated taking into account the magnetic field effect. Using similarity variable transformations, the governing equations are reduced to a set of nonlinear differential equations. Numerical results provide dual solutions in terms of the velocity ratio parameter. For increasing the volume fraction of Cu nanoparticles, magnetic field parameter, vortex viscosity parameter and magnitude of the unsteadiness parameter, the results show an increase in the local friction factor and the local couple-stress and a decrease in the local Nusselt number. On the contrary, all of these quantities significantly increase with the suction parameter. The critical values of the velocity ratio parameter, local friction factor, local couple-stress and local Nusselt number are expressed as a function of the pertinent parameters. Moreover, the thicknesses of the momentum and thermal boundary layers shrink for higher values of the suction parameter and lower values of the vortex viscosity parameter.

#### Author Contributions

Nepal Chandra Roy developed the mathematical modeling, scheme, code of the problem and examined theory validation; Md. Anwar Hossain suggested to develop the mathematical modeling and code of the problem; Ioan Pop suggested to find dual solutions, develop the mathematical modeling and examined the theory validation. The manuscript was written through the contribution of all authors. All authors discussed the results, reviewed, and approved the final version of the manuscript.

#### Conflict of Interest

The authors declared no potential conflicts of interest with respect to the research, authorship, and publication of this article.






## References

- [1] Izadi, M., Mohammadi, S. A., Mehryan, S.A.M., Yang, T. F., Sheremet, M. A., Thermogravitational convection of magnetic micropolar nanofluid with coupling between energy and angular momentum equations, *International Journal of Heat and Mass Transfer*, 145, 2019, 118748.
- [2] H. Hashemi, Z. Namazian, S.A.M. Mehryan, Cu-water micropolar nanofluid natural convection within a porous enclosure with heat generation, *Journal of Molecular Liquids*, 236, 2017, 48–60.
- [3] Hashemi, H., Namazian, Z., Zadeh, S. M. H., Mehryan, S.A.M., MHD natural convection of a micropolar nanofluid flowing inside a radiative porous medium under LTNE condition with an elliptical heat source, *Journal of Molecular Liquids*, 271, 2018, 914–925..
- [4] Bourantas, G. C., Loukopoulous, V. C., Modeling the natural convective flow of micropolar nanofluids, *International Journal of Heat and Mass Transfer*, 68, 2014, 35–41.
- [5] Bourantas, G. C., Loukopoulous, V. C., MHD natural-convection flow in an inclined square enclosure filled with a micropolar-nanofluid, *International Journal of Heat and Mass Transfer*, 79, 2014, 930–944.
- [6] Lok, Y.Y., Amin, N., Pop, I., Unsteady boundary layer flow of a micropolar fluid near the rear stagnation point of a plane surface, *International Journal of Thermal Sciences*, 42, 2003, 995–1001.
- [7] Lok, Y.Y., Amin, N., Campean, D., Pop, I., Steady mixed convection flow of a micropolar fluid near the stagnation point on a vertical surface, *International Journal of Numerical Methods for Heat & Fluid Flow*, 15, 2005, 654–670.
- [8] Hussain, S.T., Nadeem, S., Haq, R.U., Model-based analysis of micropolar nanofluid flow over a stretching surface, *The European Physical Journal Plus*, 129, 2014, 161.
- [9] Patel, H. R., Mittal, A. S., Darji, R. R., MHD flow of micropolar nanofluid over a stretching/shrinking sheet considering radiation, *International Communications in Heat and Mass Transfer*, 108, 2019, 104322.
- [10] Hussanan, A., Salleh, M. Z., Khan, I., Shafie, S., Convection heat transfer in micropolar nanofluids with oxide nanoparticles in water, kerosene and engine oil, *Journal of Molecular Liquids*, 229, 2016, 482–488.
- [11] Ishak, A., Nazar, R., Pop, I., Boundary-layer flow of a micropolar fluid on a continuous moving or fixed surface, *Canadian Journal of Physics*, 84(5), 2006, 399–410.
- [12] Bhattacharyya, K., Mukhopadhyay, S., Layek, G. C., Pop, I., Effects of thermal radiation on micropolar fluid flow and heat transfer over a porous shrinking sheet, *International Journal of Heat and Mass Transfer*, 55, 2012, 2945–2952.
- [13] Hsiao, K. L., Micropolar nanofluid flow with MHD and viscous dissipation effects towards a stretching sheet with multimedia feature, *International Journal of Heat and Mass Transfer*, 112, 2017, 983–990.
- [14] Chamkha, A. J., MHD-free convection from a vertical plate embedded in a thermally stratified porous medium with Hall effects, *Applied Mathematical Modelling*, 21, 1997, 603–609.
- [15] Krishna, M. V., Chamkha, A. J., Hall and ion slip effects on MHD rotating boundary layer flow of nanofluid past an infinite vertical plate embedded in a porous medium, *Results in Physics*, 15, 2019, 102652.
- [16] Yasin, M. H. M., Anuar Ishak, A., Pop, I., MHD stagnation-point flow and heat transfer with effects of viscous dissipation, joule heating and partial velocity slip, *Scientific Reports*, 5, 2015, 17848.
- [17] Najib, N., Bachok, N., Arifin, N. M., Ishak, A., Stagnation point flow and mass transfer with chemical reaction past a stretching/shrinking cylinder, *Scientific Reports*, 4, 2014, 4178.
- [18] Waini, I., Ishak, A., Pop, I., Hybrid nanofluid flow and heat transfer over a nonlinear permeable stretching/shrinking surface, *International Journal of Numerical Methods for Heat & Fluid Flow*, 29(9), 2019, 3110–3127.
- [19] Waini, I., Ishak, A., Pop, I., Hybrid nanofluid flow induced by an exponentially shrinking sheet, *Chinese Journal of Physics*, 2019. doi: <https://doi.org/10.1016/j.cjph.2019.12.015>
- [20] Devi, S.S.U., Devi, S.P.A., Heat transfer enhancement of Cu-Al<sub>2</sub>O<sub>3</sub>/water hybrid nanofluid flow over a stretching sheet, *Journal of Nigerian Mathematical Society*, 36, 2017, 419–433.
- [21] Lund, L. A., Omara, Z., Khan, I., Seikh, A. H., Sherif, E.-S. M., Nisar, K.S., Stability analysis and multiple solution of Cu-Al<sub>2</sub>O<sub>3</sub>/H<sub>2</sub>O nanofluid contains hybrid nanomaterials over a shrinking surface in the presence of viscous dissipation, *Journal of Materials Research and Technology*, 9(1), 2020, 421–432.
- [22] M. Shamshuddin, T. Thirupathi, P.V. S. Narayana, Micropolar fluid flow induced due to a stretching sheet with heat source/sink and surface heat flux boundary condition effects, *Journal of Applied and Computational Mechanics*, 5(5), 2019, 816–826.
- [23] Al-Hanaya, A. M., Sajid, F., Abbas, N., Nadeem, S., Effect of SWCNT and MWCNT on the flow of micropolar hybrid nanofluid over a curved stretching surface with induced magnetic field, *Scientific Reports*, 10, 2020, 8488.
- [24] Sarkar, J., Ghosh, P., Adil, A., A review on hybrid nanofluids: recent research, development and applications, *Renewable and Sustainable Energy Reviews*, 43, 2015, 164–177.
- [25] Sidik, N.A., Adamu, I.M., Jamil, M.M., Kefayati, G.H., Mamat, R., Najafi, G., Recent progress on hybrid nanofluids in heat transfer applications: a comprehensive review, *International Journal of Heat and Mass Transfer*, 78, 2016, 68–79.
- [26] Sundar, L.S., Sharma, K.V., Singh, M.K., Sousa, A.C., Hybrid nanofluids preparation, thermal properties, heat transfer and friction factor—a review, *Renewable and Sustainable Energy Reviews*, 68, 2017, 185–198.
- [27] Babu, J.R., Kumar, K.K., Rao, S.S., State-of-art review on hybrid nanofluids, *Renewable and Sustainable Energy Reviews*, 77, 2017, 551–65.
- [28] Huminic, G., Huminic, A., Hybrid nanofluids for heat transfer applications – A state-of-the-art review, *International Journal of Heat and Mass Transfer*, 125, 2018, 82–103.
- [29] Sajid, M.U., Ali, H.M., Thermal conductivity of hybrid nanofluids: a critical review, *International Journal of Heat and Mass Transfer*, 126, 2018, 211–234.
- [30] Butcher, J. C., Implicit Runge-Kutta processes, *Mathematics of Computation*, 18, 1964, 50–64.
- [31] Naschtsheim, P. R., Sweigert, P., Satisfaction of asymptotic boundary conditions in numerical solution of systems of non-linear equation of boundary layer type, NASA TN D-3004, 1965.

## ORCID iD

Nepal Chandra Roy  <https://orcid.org/0000-0002-5623-9614>

Md. Anwar Hossain  <https://orcid.org/0000-0002-3929-6211>



© 2020 by the authors. Licensee SCU, Ahvaz, Iran. This article is an open access article distributed under the terms and conditions of the Creative Commons Attribution-NonCommercial 4.0 International (CC BY-NC 4.0 license) (<http://creativecommons.org/licenses/by-nc/4.0/>).

How to cite this article: Roy, N. C., Hossain, M. A., Pop, I. Analysis of Dual Solutions of Unsteady Micropolar Hybrid Nanofluid Flow over a Stretching/Shrinking Sheet, *J. Appl. Comput. Mech.*, 7(1), 2021, 19–33. <https://doi.org/10.22055/JACM.2020.34686.2457>

